In Silico Screening of Mutational Effects on Transmembrane Helix Dimerization: Insights from Rigid-Body Docking and Molecular Dynamics Simulations

Daniele Dell'Orco,[†,‡] Pier Giuseppe De Benedetti,[†] and Francesca Fanelli*[,†,‡]

Department of Chemistry and Dulbecco Telethon Institute, University of Modena and Reggio Emilia, via Campi 183, 41100 Modena, Italy

Received: February 18, 2007; In Final Form: April 29, 2007

In this study, a docking-based protocol has been probed for its ability to predict the effects of 32 single and double mutations on glycophorin A (GpA) homodimerization. Rigid-body docking simulations have been paralleled by molecular dynamics (MD) simulations in implicit membrane. The rigid-body docking-based approach proved effective in reconstituting the native architecture of the GpA dimer for the wild type and the wild-type-like mutants. The good correlative models between the intermolecular interaction descriptors derived both by rigid-body docking simulations and by MD simulations and experimental relative free energies support the assumption that the mutation-induced changes in the association free energy of GpA helices are essentially ascribed to differences in the packing interactions, whereas almost all the variations in the entropic contributions to the association free energy are constant and/or negligible. The MD-based models achieved provide insights into the structural determinants for disruptive and restoring mutational effects. The computational approaches presented in this study are fast and effective, and constitute simple and promising tools for in silico screening of mutational effects on the association properties of integral membrane proteins.

Introduction

The association of helices within the apolar milieu of lipidic bilayers is an attractive issue for several reasons. One reason is that helix−helix interactions are considered the last crucial step of the membrane protein folding mechanism[1−4] according to the widely accepted two-stage folding model.[5,6] Another reason is that increasing evidence is emerging about the importance of membrane protein oligomerization in the regulation of a variety of biochemical processes.

Homooligomeric transmembrane helices are particularly attractive systems for the study of membrane protein folding and stability. Indeed, the noncovalent assembly of membrane peptides is likely to mimic the folding of larger native proteins, as demonstrated by various fragment-complementation studies (see refs 1 and 4 and references therein). Among such systems, glycophorin A (GpA) homodimer from erythrocyte membrane represents one of the most studied cases to date. High-resolution structural data from solution NMR in dodecylphosphocholine (DPC) micelles[7] and from solid-state NMR in dimyristoylphosphatidylcholine (DMPC) bilayers,[8,9] together with the plenty of mutagenesis work aimed at characterizing the thermodynamics of association,[10−16] make this system intriguing for computational studies of helix−helix associations.

Recently, we set up a computational protocol based upon rigid-body docking for fast predictions of mutational effects on the thermodynamics of association of a number of protein−protein complexes. So far, the method has been used on a total of 67 heterogeneous variants of water-soluble protein−protein complexes,[17,18] and on 10 mutants of the MEF2A transcription factor in complex with DNA.[19] The fundamental requirement of the approach is an accurate structural model of the complex between the wild type forms of the interacting macromolecules. The variants (i.e., mutations or deletions) of either partner or both partners can be achieved by molecular modeling. The basic assumption is that the architecture of the mutated complexes is almost the same as that of the wild type and no major conformational changes occur upon binding.

The good performance of the method is related to the scoring function of the protein−protein docking algorithm ZDOCK,[20−22] which effectively accounts for electrostatic and shape complementarities as well as desolvation. We have also shown that neglecting the desolvation term in docking simulations leads to effective quaternary structure predictions of oligomeric membrane proteins, independent of the oligomeric order and of the extension of the intracellular and extracellular hydrophilic domains.[23]

In this study, we test the same docking-based protocol in its ability to predict the effects of 32 single and double mutations on GpA homodimerization, hence reproducing in silico a set of in vitro alanine-scanning mutagenesis experiments done in recent years.[11−14] Rigid-body docking simulations have been paralleled by molecular dynamics (MD) simulations in implicit membrane.[24] The input structures for such simulations were the wild type and 32 mutated forms of the solid-state NMR structure.[8,9]

The results of this study corroborate the effectiveness of our rigid-body docking-based protocol in fast estimation of mutational effects on the thermodynamics of protein−protein association, independent of the environment, i.e., water or membrane. Moreover, combining the results of rigid-body docking with MD simulations add interpretative power to the correlative models.

Methods

Rigid-Body Docking Simulations of GpA Dimerization. Rigid-body docking simulations of GpA homodimerization were carried out by means of the rigid-body docking algorithm

* Corresponding author. Telephone: +39 059 2055114. Fax: +39 059 373543. E-mail: fanelli@unimo.it.
† University of Modena and Reggio Emilia.
‡ Dulbecco Telethon Institute.

10.1021/jp071383r CCC: $37.00
Published on Web 06/28/2007

TABLE 1: GpA Dimerization: In Vitro Thermodynamic Data and Structural Parameters from Rigid-Body Docking and Molecular Dynamics Simulations

variant	$\Delta\Delta G°_{exp}$[a] (kcal/mol)	$\Delta G°_{coup}$[b] (kcal/mol)	ΔZD[c]	cluster population[d]	best rank[e]	ZD^{best}[f]	ΔIE_1[g] (kcal/mol)	C_α-rmsd$_1$[h] (Å)	ΔIE_2[i] (kcal/mol)	C_α-rmsd$_2$[j] (Å)
wt	0.0 ± 0.1	0	0.00 ± 0.05	58, 61, 59 (179)	3, 21, 7	8.08, 7.52, 7.84	0.00	0.82	0.00	0.66
L75A	1.3 ± 0.1	0	0.04 ± 0.05	67, 70, 70 (207)	1, 1, 3	8.32, 8.46, 8.16	5.27	1.51	3.20	0.66
I76A	1.8 ± 0.2	0	−0.04 ± 0.05	57, 52, 56 (165)	6, 4, 9	8.30, 8.04, 8.14	9.15	1.5	4.44	0.97
I77A	0.0 ± 0.1	0	−0.20 ± 0.05	59, 57, 56 (172)	4, 8, 2	8.48, 7.96, 8.54	0.71	1.66	−0.58	1.03
F78A	0.0 ± 0.1	0	−0.14 ± 0.05	62, 59, 62 (183)	2, 3, 2	8.22, 8.02, 8.86	1.29	0.71	0.19	1.39
G79A	1.7 ± 0.1	0	0.35 ± 0.05	41, 43, 35 (119)	13, 41, 34	7.70, 7.14, 7.14	12.23	1.09	7.52	1.14
V80A	0.4 ± 0.1	0	0.05 ± 0.04	49, 47, 50 (146)	6, 17, 5	8.16, 7.74, 8.40	15.53	1.08	2.33	1.62
M81A	−0.1 ± 0.1	0	−0.11 ± 0.05	55, 66, 60 (181)	4, 4, 1	8.02, 8.14, 8.48	3.18	1.48	−1.47	1.48
G83A	3.1 ± 0.1	0	0.60 ± 0.04	33, 30, 34 (97)	172, 51, 153	6.60, 7.08, 6.70	14.62	2.22	15.42	
V84A	1.0 ± 0.1	0	0.04 ± 0.04	47, 46, 50 (143)	6, 2, 14	7.94, 8.24, 7.62	2.95	1.57	−3.14	1.20
I85A	−0.2 ± 0.1	0	−0.07 ± 0.05	53, 59, 51 (163)	9, 24, 8	7.96, 7.68, 8.00	2.52	1.5	0.00	1.33
G86A	−0.4 ± 0.1	0	−0.10 ± 0.04	63, 66, 63 (192)	1, 2, 3	8.42, 8.00, 7.96	−0.71	1.65	−1.58	1.05
T87A	0.9 ± 0.1	0	0.21 ± 0.05	45, 36, 32 (113)	15, 17, 66	7.98, 7.64, 7.14	0.00	1.26	0.80	
L75A/I76A	2.4 ± 0.1	−0.7	0.08 ± 0.04	49, 49, 48 (146)	9, 15, 2	7.96, 7.70, 8.10	14	1.6	5.71	1.06
L75A/G79A	2.3 ± 0.1	−0.7	0.36 ± 0.04	45, 45, 40 (130)	67, 49, 27	7.06, 7.26, 7.42	18.15	1.58	9.42	1.53
L75A/V80A	1.3 ± 0.3	−0.4	−0.01 ± 0.04	63, 52, 66 (181)	5, 5, 10	8.20, 8.28, 7.86	14.78	1.07	6.88	1.46
L75A/G83A	3.6 ± 0.2	−0.8	0.55 ± 0.05	22, 21, 23 (66)	57, 57, 128	6.96, 6.92, 6.72	21.69	1.75	22.49	
L75A/V84A	0.1 ± 0.1	−2.2	0.12 ± 0.04	66, 63, 61 (190)	7, 11, 8	7.94, 7.86, 7.90	13.05	1.21	1.08	1.46
I76A/G79A	2.9 ± 0.2	−0.6	0.36 ± 0.04	40, 42, 43 (125)	26, 19, 29	7.24, 7.30, 7.22	17.2	1.53	8.63	1.22
I76A/V80A	2.5 ± 0.3	0.3	0.04 ± 0.05	49, 45, 48 (142)	14, 24, 13	7.94, 7.80, 7.96	15.16	1.33	7.89	1.49
I76A/G83A	3.4 ± 0.2	−1.6	0.77 ± 0.04	24, 21, 26 (71)	97, 132, 280	6.76, 6.58, 6.32	18.9	2.5	19.70	
I76A/V84A	1.2 ± 0.1	−1.6	0.07 ± 0.04	51, 47, 51 (149)	6, 11, 15	7.92, 7.60, 7.66	13.59	1.5	4.01	1.36
I76A/T87A	2.8 ± 0.2	0.1	0.50 ± 0.04	40, 36, 40 (116)	34, 75, 107	7.26, 6.90, 6.80	13.34	1.29	14.14	
G79A/V80A	2.4 ± 0.1	0.3	0.56 ± 0.04	32, 34, 29 (95)	62, 108, 62	6.96, 6.70, 6.94	17.19	1.47	9.07	0.93
G79A/G83A	3.6 ± 0.3	−1.2	0.62 ± 0.04	28, 25, 23 (76)	85, 101, 168	6.80, 6.66, 6.54	14.37	2.02	15.17	
G79A/V84A	3.0 ± 0.2	0.3	0.48 ± 0.04	29, 34, 33 (96)	14, 29, 45	7.52, 7.18, 7.04	17.7	1.39	5.85	1.36
G79A/T87A	2.8 ± 0.2	0.2	0.25 ± 0.06	30, 27, 22 (79)	20, 15, 35	7.66, 7.64, 7.40	16.13	1.55	16.93	
V80A/G83A	3.5 ± 0.1	0	0.73 ± 0.03	20, 18, 20 (58)	884, 413, 499	6.00, 6.30, 6.22	14.96	1.58	15.76	
V80A/V84A	2.0 ± 0.2	0.6	−0.06 ± 0.05	47, 45, 45 (137)	3, 27, 5	8.42, 7.62, 8.12	11.45	1.57	0.11	1.57
V80A/T87A	3.7 ± 0.2	2.4	0.27 ± 0.04	35, 34, 38 (107)	17, 61, 54	7.74, 7.24, 7.34	9.64	1.27	10.44	
G83A/V84A	3.2 ± 0.1	−0.9	0.55 ± 0.06	13, 16, 15 (44)	116, 115, 90	6.76, 6.78, 6.88	14.52	1.61	13.41	
G83A/T87A	3.3 ± 0.1	−0.7	0.78 ± 0.07	14, 9, 12 (35)	47, 240, 269	7.16, 6.46, 6.44	15.69	3.16	16.49	
V84A/T87A	1.0 ± 0.1	−0.9	0.25 ± 0.06	38, 34, 33 (105)	7, 52, 21	8.16, 7.40, 7.76	6.06	1.38	6.86	

[a] Experimental changes of binding free energy of GpA dimerization upon mutation, defined by the relationship $\Delta\Delta G° = \Delta G°_{mut} - \Delta G°_{wt}$.[11−14] Here and in the following definitions, "mut" refers to the mutated GpA form, while "wt" refers to the wild type dimer. [b] Free energy of coupling, as defined in eq 2 in the text. [c] Relative average docking scores for the nativelike complexes obtained from three independent docking runs, defined by the relationship $\Delta ZD = ZD\text{-}s_{mut} - ZD\text{-}s_{wt}$. The standard errors are reported. [d] Number of nativelike solutions obtained from each independent docking run, out of 4000 overall configurations saved for each run. Data referred to each run are separated by commas. In parentheses is reported the population of each nativelike ensemble used in correlation analyses, out of 12 000 overall retained configurations. [e] Rank order of the best-scored nativelike solution resulting from each run out of 4000 overall retained configurations. Commas separate data from each run. [f] ZDOCK score of the best-scored nativelike solution resulting from each run out of 4000 overall retained configurations. Commas separate data from each run. [g] Changes in the interaction energy with respect to the wild type defined by the relationship $\Delta IE_1 = IE_1^{mut} - IE_1^{wt}$. The interaction energies have been computed on the average minimized structures of the wild type and mutated forms derived by MD simulations in the absence of interhelical distance restraints between the hydroxy oxygen atom of T87 from one helix and the backbone oxygen atom of V84 from the other helix. [h] α-Carbon root-mean-square deviation between the average minimized structure obtained by 1 ns MD simulation without interhelical distance restraints and the experimental solid-state NMR structure.[9] [i] Changes in the interaction energy with respect to the wild type defined by the relationship $\Delta IE_2 = IE_2^{mut} - IE_2^{wt}$. For the wild type and all mutants except for the G83A and T87A series, the interaction energies have been computed on the average minimized structures derived by MD simulations in the presence of interhelical distance restraints between the hydroxy oxygen atom of T87 from one helix and the backbone oxygen atom of V84 from the other helix. [j] α-Carbon root-mean-square deviation between the average minimized structure obtained by 1 ns MD simulation with interhelical distance restraints and the experimental solid-state NMR structure.[9]

ZDOCK2.1.[20,21] The grid-based pairwise scoring function[22] implemented in this version of the software accounts for shape and electrostatic complementarities neglecting the desolvation term, which is suitable for aqueous environments. The algorithm performs an efficient fast Fourier transform sampling of the entire six degrees of freedom in the translational and rotational space, and finally provides a score for each docking solution, which is representative of the complementarity of the complex.

Docking simulations were carried out on the wild type and 32 single and double mutant forms (Table 1). Truncated forms of segments A and B corresponding to the transmembrane portions (i.e., I76-I95 segments) were considered for docking simulations. Both the solid-state NMR structure in DMPC bilayers[8,9] and the minimized structure averaged over the 20 structures resolved by solution NMR in DPC micelles[7] were initially employed to extract the I76-I95 A and B segments. However, the solid-state NMR structure was finally selected for the gross of rigid-body docking simulations and analysis as well as for MD simulations (see the following section). The rationale behind the choice of the solid-state NMR structure instead of the solution structure was the more extended interface in the former compared to the latter and the consequent best performance of the docking algorithm. A posteriori, this choice is supported by the results of MD simulations in DPC micelle and DMPC bilayer, which converged in a helix−helix packing architecture similar to that of the NMR structure determined in bilayer.[25] Single and double Ala mutations (Table 1) in both monomers were performed by means of the Protein Design module within the QUANTA2005 package.

Three independent sets of docking runs were performed for each complex, i.e., one starting from the experimental coordinates and the other two randomizing the initial positions of the probe, in a fashion previously described.[18] A 128 × 128 × 128 point grid with a 1.2 Å spacing was used for digitalizing the

interacting molecules. In each docking run, the GpA monomer corresponding to segment A was kept fixed (i.e., target), whereas the one corresponding to segment B was allowed to rotate and translate around the target (i.e., probe). A rotational sampling interval of 6° was employed, i.e., dense sampling, and the best 4000 solutions were retained for each run and ranked according to their score. As for docking analysis, according to previous work,[17,18,26] we selected as nativelike structures all the docked complexes characterized by an α-carbon atom root-mean-square deviation (C_α-rmsd) less than 1.0 Å from the native complex. For each molecular system, we considered the ZDOCK score averaged over the scores of all the nativelike complexes resulting from the three independent runs and constituting the nativelike ensemble. These average scores (ZD-s) were then employed in the correlation analysis with thermodynamic data. In detail, correlations were carried out between the relative ZD-s (ΔZD), i.e., the difference between the ZD-s of a given form and that of the wild type, and the relative binding affinity ($\Delta\Delta G°$), i.e., the difference between the $\Delta G°$ of a given form and that of the wild type (Table 1 and references therein). The wild type form has ΔZD-s and $\Delta G°$ values equal to 0.

Molecular Dynamics Simulations of GpA Dimers. MD simulations were carried out on the solid-state NMR structure in its wild type and 32 mutated forms. Alanine replacements were made on both chains A and B in the GpA dimer by means of the CHARMM program.[27] Such input structures of the wild type and of the mutants that differ only for the mutated side chains were, thus, subjected to energy minimization and MD simulations, by using the GBSW implicit membrane/water model recently implemented in CHARMM (i.e., c32b1 version).[28] The all-hydrogen parameter set PARAM22/CMAP of the CHARMM force field was used. No cutoff was used for the nonbonded energy evaluation. A smoothing length of 0.6 Å ($w = 0.3$ Å) was employed in both PB and GB calculations, by setting $a_0 = -0.180$, $a_1 = 1.817$, and $s = 0.952$. As for the physical parameters representing the membrane in the GB model, the surface tension coefficient (representing the nonpolar solvation energy) was set to 0.03 kcal/(mol·Å^2). Furthermore, the membrane thickness centered at $Z = 0$ was set to 29.0 Å with a membrane smoothing length of 5.0 Å ($w_m = 2.5$ Å).

Minimizations were carried out by using 500 steps of steepest descent followed by adopted basis Newton−Raphson (ABNR) minimization, until the root-mean-square gradient was less than 0.001 kcal/(mol·Å). MD production phases consisted in 1 ns of Langevin dynamics at 300 K with a friction coefficient of 5.0 ps^{-1}. The lengths of the bonds involving the hydrogen atoms were restrained by the SHAKE algorithm, allowing for an integration time step of 0.001 ps.

The secondary structure of the two helices was preserved by assigning distance restraints (i.e., minimum and maximum allowed distances of 2.7 and 3.0 Å, respectively) between the backbone oxygen atom of residue i and the backbone nitrogen atom of residue i + 4. The scaling factor of such restraints was 10, and the force constant at 300 K was 10 kcal/(mol·Å). An equivalent set of MD simulations was also carried out by imposing interhelical distance restraints between the hydroxy hydrogen atom of T87 (i.e., HG1) and the backbone oxygen atom of V84 (i.e., O). These additional simulations were carried out on the minimized coordinates of the wild type and of all the mutants holding the interhelical H-bonds involving T87. Such a set of mutants excludes all the alanine substitutions for T87 and the alanine substitutions for G83, taken singularly or paired with alanine replacements of L75, I76, G79, V80, and V84 (Table 1).

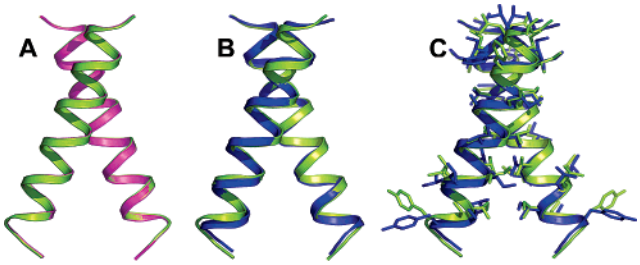

Figure 1. Structural predictions of wild type GpA dimerization. (A) Cartoon representation of the best-scored docking solution, i.e., solution N.3 from the first docking run (magenta), superimposed on the native solid-state NMR structure (green). The C_α-rmsd between the two structures is 0.16 Å. (B) Cartoon representation of the minimized structure averaged over the 2000 structures constituting the 1 ns MD trajectory (blue) superimposed on the solid-state NMR structure (green). The C_α-rmsd between the two structures is 0.82 Å. (C) Same representation as in (B), in which the amino acid side chains are represented by sticks.

The MD setup reported above was selected from among a large number of trial runs, because it was the one that better maintained the structure of wild type GpA. Trial tests included also the probing of (a) different positions of the input structure relative to the membrane center, (b) different membrane thicknesses (i.e., 25, 30, and 32 Å), (c) different friction coefficients for the Langevin dynamics (i.e., 0.5 and 10 ps^{-1}), (d) Nose−Hoover dynamics at 300 K with and without intrahelix distance restraints, (e) Langevin dynamics without intrahelix distance restraints, and (f) finite cutoffs for the nonbonded interactions.

The structures of the wild type and of the mutants averaged over the 1 ns equilibrated trajectories were considered for the structural and correlative analyses.

The interaction energies, IE (i.e., the total energy of the helix−helix complex minus the energy of each helix in the complex), were computed both on each frame and on the average minimized structures. The difference between the IE of a given GpA form and that of the wild type (i.e., relative IE or ΔIE) was considered for the correlative analyses. By definition, the ΔIE of the wild type is equal to 0.

Results

Rigid-Body Docking Simulations of GpA Dimerization: Output Analyses. Three sets of repeated and independent rigid-body docking simulations were run to reproduce GpA dimers in their native and 32 mutated forms. Data concerning both relative affinities as determined by analytical ultracentrifugation experiments[11,13,14] and relative docking scores are reported in Table 1. The basic assumption of the approach is that mutated GpA dimers hold almost the same architecture as the wild type form. In this respect, for each variant, the docking algorithm was able to reproduce nativelike dimers with a ranking number strictly related to the binding affinity. In detail, for each independent run concerning the wild type form, a nativelike solution was found within the best-scored 21 solutions out of the 4000 saved configurations (Table 1). The best-scored solution, i.e., solution N.3 from the first run (Table 1), holds a C_α-rmsd from the native solid-state NMR structure[8,9] equal to 0.16 Å (Figure 1A). Similar results were achieved for all the wild-type-like mutants, as far as binding affinity is concerned (Table 1). Interestingly, the relative population of the nativelike ensemble, i.e., the ensemble of all the nativelike solutions from each independent docking run, correlates linearly both with the relative binding free energy, $\Delta\Delta G°$ ($N = 33$, $R = 0.81$, $p <$

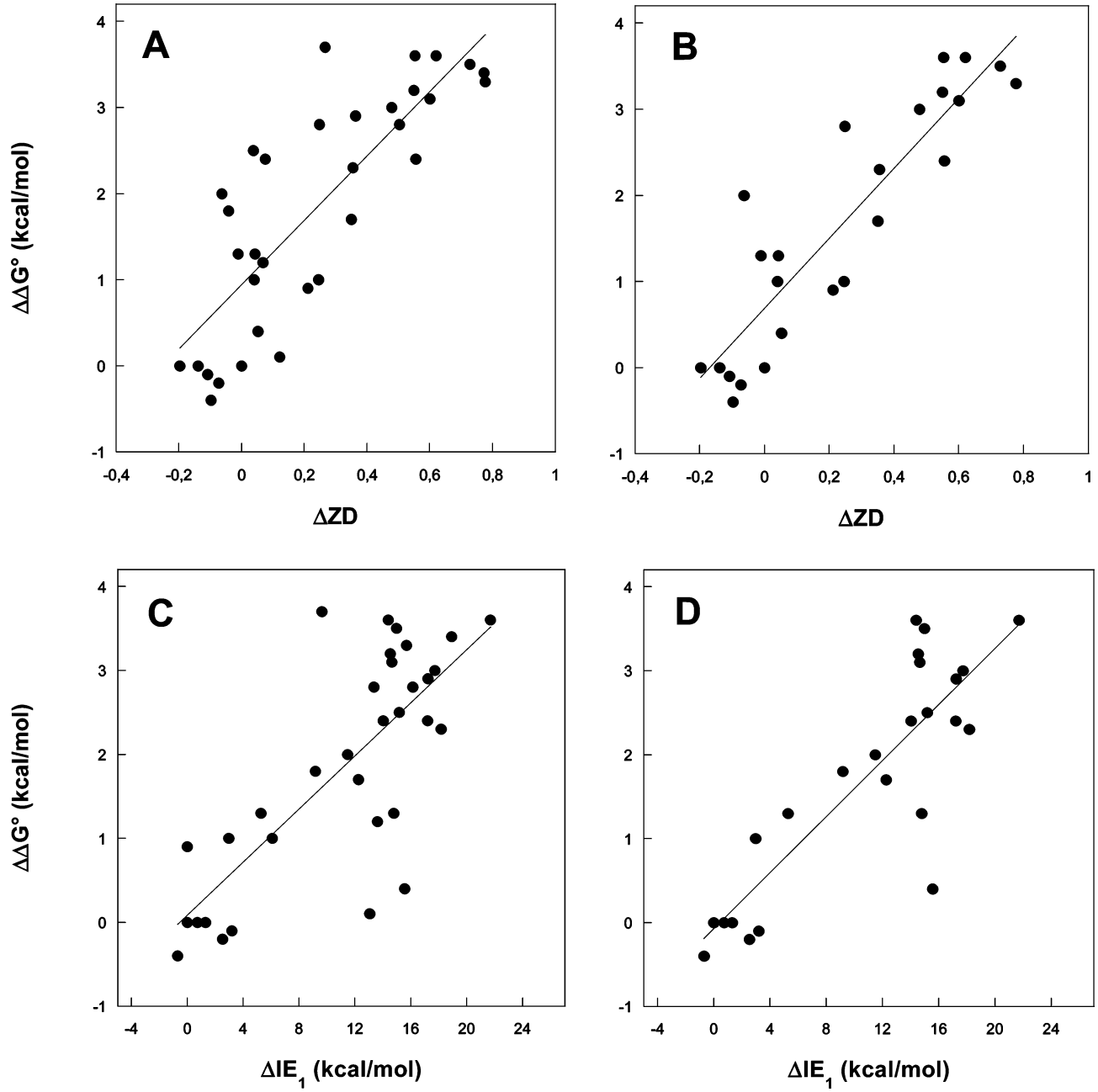

Figure 2. Correlative models for the prediction of mutational effects on GpA homodimerization. The correlation between relative affinities ($\Delta\Delta G°$) and relative docking scores (ΔZD) is shown by considering (A) the whole set of data values ($\Delta\Delta G° = 0.9(\pm0.2) + 3.7(\pm0.5)\Delta$ZD; $N = 33$, $R = 0.82$, $p < 0.0001$, $s = 0.79$) and (B) leaving out the outliers ($\Delta\Delta G° = 0.7(\pm0.2) + 4.1(\pm0.4)\Delta$ZD; $N = 24$, $R = 0.90$, $p < 0.0001$, $s = 0.62$). The correlation between relative affinities and relative interaction energies (ΔIE_1) computed on the average minimized complexes of the wild type and the mutants is shown by considering (C) the whole set of data values ($\Delta\Delta G° = -0.1(\pm0.3) + 0.16(\pm0.02)\Delta IE_1$; $N = 33$, $R = 0.77$, $p < 0.0001$, $s = 0.87$) and (D) by omitting the outliers ($\Delta\Delta G° = -0.1(\pm0.3) + 0.17(\pm0.02)\Delta IE_1$; $N = 24$, $R = 0.85$, $p < 0.0001$, $s = 0.73$).

0.001, and $s = 0.79$, where N is the number of data points, R is the correlation coefficient, p is the R probability, and s is the standard deviation), and with the ΔZD ($N = 33$, $R = 0.88$, $p < 0.001$, $s = 0.14$) of each nativelike ensemble. These correlations are apparently independent of the number of docking runs and of the C_α-rmsd threshold selected to define the nativelike ensemble. This inference is supported, at least in part, by the lack of correlation ($R = 0.25$) between the relative populations of each nativelike ensemble and the standard errors of the ZD scores of each member of such ensembles (Table 1).

Rigid-Body Docking Simulations of GpA Dimerization: Building Quantitative Models for Estimating Mutational Effects on the Thermodynamics of Helix−Helix Association. A significant correlation was found between relative binding affinities ($\Delta\Delta G°$) and relative ZD-s (ΔZD) of the wild type and of the 32 GpA mutants. The latter are single and double alanine replacements located in both interacting helices (i.e., segments A and B in the GpA homodimer). When all the points are considered, the linear correlation equation obtained is (Figure 2A)

$$\Delta\Delta G° = 0.9(\pm0.2) + 3.7(\pm0.5)\Delta\text{ZD};\quad N = 33,\ R = 0.82,\ p < 0.0001,\ s = 0.79 \quad (1)$$

Nine points are outliers in this equation. They can be divided in two sets. The first set of outliers comprises the seven single and double mutants involving I76, whereas the second set is made of the L75A/V84A and V80A/T87A mutants, which share

a strong free energy of coupling (ΔG°_{coup}) with respect to the individual effects of the single mutations. ΔG°_{coup} of a double mutant is defined by the following formula:

$$\Delta G^\circ_{coup} = \Delta\Delta G^\circ_{mut1mut2} - (\Delta\Delta G^\circ_{mut1} + \Delta\Delta G^\circ_{mut2}) \quad (2)$$

where $\Delta\Delta G^\circ_{mut1}$ and $\Delta\Delta G^\circ_{mut2}$ are the relative free energies of the single mutants and $\Delta\Delta G^\circ_{mut1mut2}$ is the relative free energy of the double mutant resulting from the combination of the two single mutants.

As for the first set of outliers, the ZD-s predicts a wild-type-like behavior for the mutants involving I76, inconsistent with in vitro evidence (Table 1). This may be due, at least in part, to the fact that the location of I76 is such that the packing interactions of this amino acid residue are strongly affected by the tilt angle of the interacting helices. In fact, the packing interactions of I76 are different in the solid-state and solution NMR structures, which differ in the helix tilt angle (i.e., 35° and 40°, respectively).[7−9] In line with these data, we have observed that, when docking simulations and analysis are carried out on the wild type and mutated monomers extracted from the minimized structures averaged over the 20 structures obtained by solution NMR,[7] the ZDOCK score better estimates the effects of I76 mutation on the binding free energy (i.e., $\Delta ZD = 0.23$). Such an improvement of the ZD-s performance when the solution NMR structure is used instead of the solid-state NMR structure concerns, however, only the mutants involving I76, in particular the I76A single mutant. A worsening of the correlative model extended to all the 33 GpA forms was, in fact, observed, compared to simulations on the solid-state NMR structure (results not shown), probably due to the significantly less extended interface in the solution NMR structure compared to the solid-state one.[7,9]

Thus, when the data points corresponding to the I76A series together with L75A/V84A and V80A/T87A are omitted from the correlation, a significant improvement in the correlation statistics is observed (Figure 2B):

$$\Delta\Delta G^\circ = 0.7(\pm 0.2) + 4.1(\pm 0.4)\Delta ZD; \quad N = 24,\ R = 0.90,\ p < 0.0001,\ s = 0.62 \quad (3)$$

When the same set of points are subjected to the leave-one-out validation test to probe the predictive capability of the model, the resulting equation is:

$$\Delta\Delta G^\circ_{exp} = 0.1(\pm 0.2) + 1.0(\pm 0.1)\Delta\Delta G^\circ_{pred}; \quad N = 24,\ R = 0.89,\ p < 0.0001,\ s = 0.65 \quad (4)$$

Molecular Dynamics Simulations of GpA Dimers: Structural Analysis. In this study, we carried out two sets of MD simulations starting from the wild type and the mutated forms of the solid-state NMR structure.[8,9] In both sets of simulations, intrahelix distance restraints were employed to reduce the degrees of freedom and effectively exploring mutational effects on the helix−helix packing, given the relatively short simulation time (1 ns). The computational setup proved able to maintain the structure of the wild type GpA dimer. In fact, the C_α-rmsd between the solid-state NMR structure and the wild type structure averaged over the 2000 structures constituting the 1 ns trajectory is 0.82 Å (Table 1) and maintains a similar value for all 2000 frames constituting the trajectory (blue line in Figure 3). Collectively, the C_α-rmsd's computed on the average minimized structures of the wild type and of the mutants correlate significantly with the C_α-rmsd's averaged over the C_α-rmsd's of each frame in the trajectory (i.e., $R = 0.93$, $p < 0.0001$). Among the single mutants, G83A shows the highest C_α-rmsd with respect to the solid-state NMR structure. This result is consistent with the fact that alanine substitution for G83 exerts the most detrimental effect on the binding free energy among the single mutants (Table 1 and Figure 3). In line with these observations, the double mutants involving G83 reach the highest C_α-rmsd values, consistent with their unfavorable effect on the binding free energy (Table 1 and Figure 3). G83A mutation is predicted to affect the overall helix−helix packing, resulting in both the loss and the weakening of native interhelical interactions (Figure 4). The structural analysis also suggests that, in general, the pairing of G83 with any other mutant attenuates the structure deviation from the solid-state NMR structure, compared to the single G83A mutant (Table 1 and Figures 3−5). An exception to this observation is represented by the G83A/T87A double mutant, which shows a structural deviation from the experimental structure higher than that of G83A (Table 1 and Figures 3 and 5). One of the structural perturbations associated with the G83A mutation is the breakage of the weak interhelical H-bond found in the solid-state NMR structure between the hydroxy hydrogen atom of T87 from one helix and the backbone oxygen atom of V84 from the other helix. Different from the T87A single and double mutants, for which such H-bond loss is the primary perturbation at the mutation site, for the G83A mutants, it is the consequence of a detachment of the backbone of the two interacting helices in proximity to the mutation site. In fact, the primary perturbations induced by alanine substitution for G83 are steric clashes between the methyl groups of A83 from both helices, and between the methyl group of A83 from one helix and the backbone atoms of V80 from the other helix. These steric clashes cause a helix−helix backbone detachment in proximity to the mutation site and the consequent loss of the interhelical H-bonds already at the minimization stage that precedes MD simulations. Different from the G83A mutants, in the other mutants considered in this study and in the wild type form, the two interhelical H-bonds are retained following energy minimization, but are always lost during MD simulations, being replaced by intrahelix H-bonds between the hydroxy oxygen atom of T87 and the carbonyl oxygen atom of G83. These data agree with the 20 dimeric GpA structures resolved by solution NMR, in which T87 performs an intrahelix H-bond rather than an interhelix one. They are also consistent with the results of MD simulations in implicit membrane/water already achieved on the same system.[28,29] However, since the input of our MD simulations is the solid-state NMR structure of the wild type and not the solution NMR structure, we investigated the role of the two interhelical H-bonds in the structure and energetics of helix−helix association. Therefore, the wild type and mutant forms, which presented such H-bonds at the energy minimization stage, were subjected to additional MD simulations by using distance restraints between the hydroxy oxygen atom of T87 from one helix and the backbone oxygen atom of V84 from the other helix. In all the GpA forms subjected to such restraints, the two interhelical H-bonds persisted over the simulation time and, therefore, were features of the structures averaged over all 2000 structures constituting the equilibrated MD trajectory. The presence of such H-bonds lowered the C_α-rmsd of the wild type from the solid-state NMR structure (i.e., from 0.82 to 0.62 Å, Table 1, Figure 6), suggesting a non-negligible structural role for these weak interhelical interactions.

Molecular Dynamics Simulations of GpA Dimers: Building a Quantitative Model for Estimating Mutational Effects on the Thermodynamics of Helix−Helix Association. In this

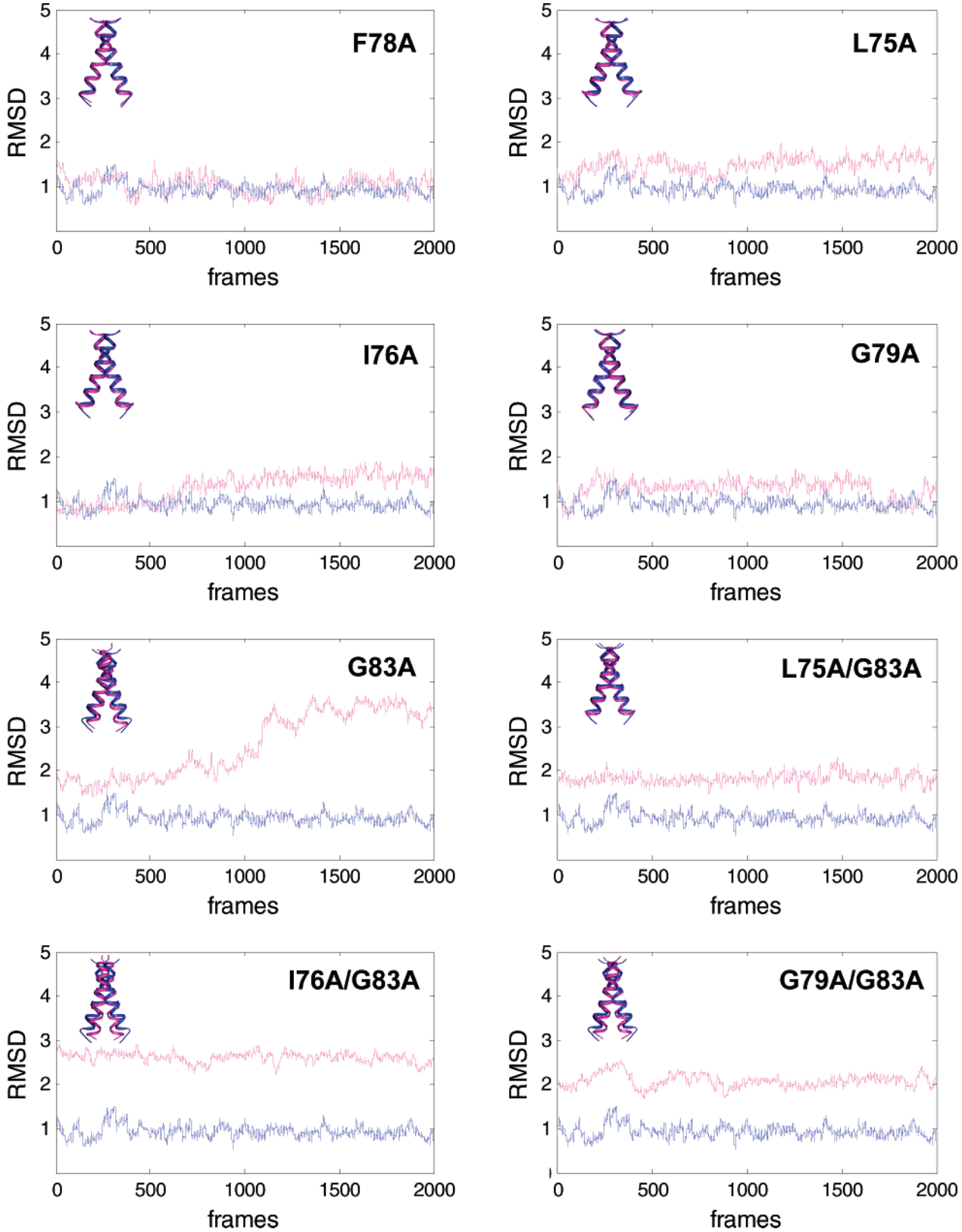

Figure 3. The 1 ns MD trajectories of wild type (blue) and mutant (magenta) forms of GpA dimers. Each panel reports the C_α-rmsd (Å) of each frame with respect to the experimental solid-state NMR structure. Each inset shows a cartoon representation of the average minimized structure of the mutant (magenta) superimposed on the NMR solid-state structure (blue).

study, we searched for descriptors computed on the MD simulated structures able to account for mutational effects on the free energies of helix−helix association. The relative interaction energies (IE) computed on the average minimized structures lacking the interhelical H-bonds involving T87 (ΔIE_1) were good in this respect (Table 1 and Figure 2). Such computational indices, which are significantly correlated with the ΔIE averaged over the 2000 structures constituting the 1 ns trajectory ($R = 0.90$), were employed for the correlation analysis. In this respect, a good linear correlation was found

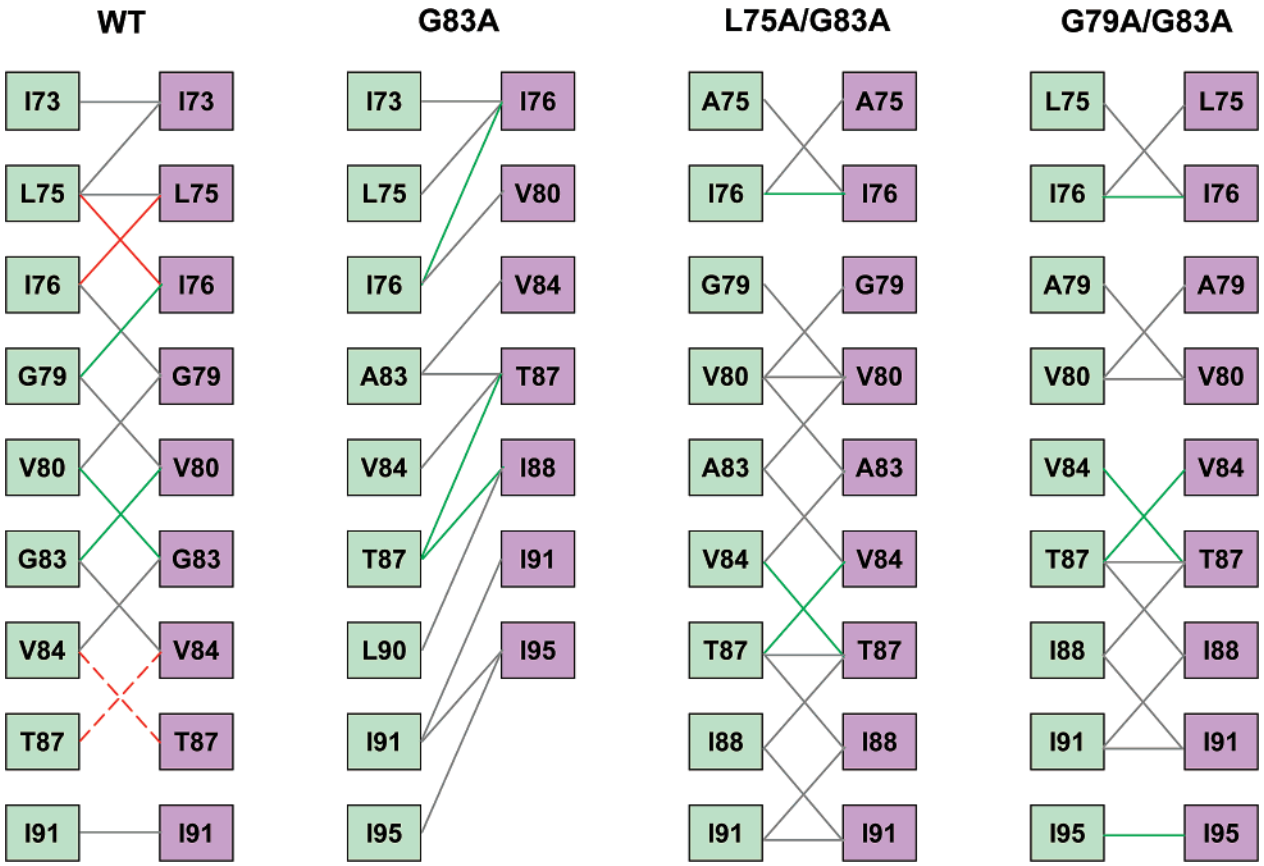

Figure 4. Amino acids that contribute to the intermonomer interface in the average minimized structures of the wild type and the G83A, L75A/G83A and G79A/G83A GpA mutants. In each diagram, green squares refer to residues belonging to the A monomer, whereas violet squares refer to the B monomer. Intermolecular interactions are represented by colored lines. In detail, gray lines refer to interactions ranging from −1 to −2 kcal/mol, green lines refer to interactions from −2 to −3 kcal/mol, and red lines refer to interactions higher than −3 kcal/mol. Dashed lines indicate interhelical hydrogen bonds.

between ΔIE_1 and $\Delta\Delta G°$. The correlation equation, by considering all together the wild type and the 32 GpA mutants, is the following (Figure 2C):

$$\Delta\Delta G° = -0.1(\pm 0.3) + 0.16(\pm 0.02)\Delta IE_1; \quad N = 33, R = 0.77, p < 0.0001, s = 0.87 \quad (5)$$

Similar to the correlative models based upon the ZD-s, two sets of outliers were found. Also, in this case, one set comprised double mutants characterized by strong $\Delta G°_{coup}$ values (namely, L75A/V84A, I76A/G83A, and I76A/V84A; Table 1). The other set comprised all the single and double mutants involving T87 (i.e., six outliers), whose effects were all underestimated by the computational index. Omitting these nine points significantly improved the correlation equation (Figure 2D):

$$\Delta\Delta G° = -0.1(\pm 0.3) + 0.17(\pm 0.02)\Delta IE_1; \quad N = 24, R = 0.85, p < 0.0001, s = 0.73 \quad (6)$$

Intriguingly, pairing ΔIE_1 with the relative C_α-rmsd's (Δrmsd) led to the following two-variable correlation equation:

$$\Delta\Delta G° = -0.2(\pm 0.3) + 0.13(\pm 0.02)\Delta IE_1 + 0.8(\pm 0.3)\Delta\text{rmsd}; \quad N = 33, R = 0.81, s = 0.81, F = 28.8 \quad (7)$$

where F is the F-test value, and to the predicted versus experimental equation:

$$\Delta\Delta G°_{exp} = 0.0(\pm 0.3) + 1.00(\pm 0.13)\Delta\Delta G°_{pred}; \quad N = 33, R = 0.81, p < 0.0001, s = 0.80 \quad (8)$$

Both these correlative models improved following deletion of the nine points discussed above. The correlation equation and the predictive model respectively became:

$$\Delta\Delta G° = -0.5(\pm 0.3) + 0.14(\pm 0.02)\Delta IE_1 + 1.2(\pm 0.4)\Delta\text{rmsd}; \quad N = 24, R = 0.90, s = 0.63, F = 42.8 \quad (9)$$

and

$$\Delta\Delta G°_{exp} = 0.0(\pm 0.2) + 1.00(\pm 0.11)\Delta\Delta G°_{pred}; \quad N = 24, R = 0.90, p < 0.0001, s = 0.62 \quad (10)$$

The unsuitability of ΔIE_1 to account for the relative effects of the T87 mutations on the free energy of GpA homodimerization was due, at least in part, to the lack of the interhelical H-bond in the structures derived without interhelical restraints simulations. In fact, recalculating the ΔIE on the wild type and the mutated structures holding the interhelical H-bonds (ΔIE_2) properly accounted for the effects of the T87 mutations, improving significantly the correlative model (Table 1 and Figure 7). The novel correlation equation, which comprises all the GpA forms except for V84A and V80A/V84A, is the following:

$$\Delta\Delta G° = -0.4(\pm 0.2) + 0.18(\pm 0.02)\Delta IE_2; \quad N = 31, R = 0.89, p < 0.0001, s = 0.63 \quad (11)$$

Discussion

The GpA homodimer has been widely used as a model system for in vitro and in silico experiments aimed at unraveling the

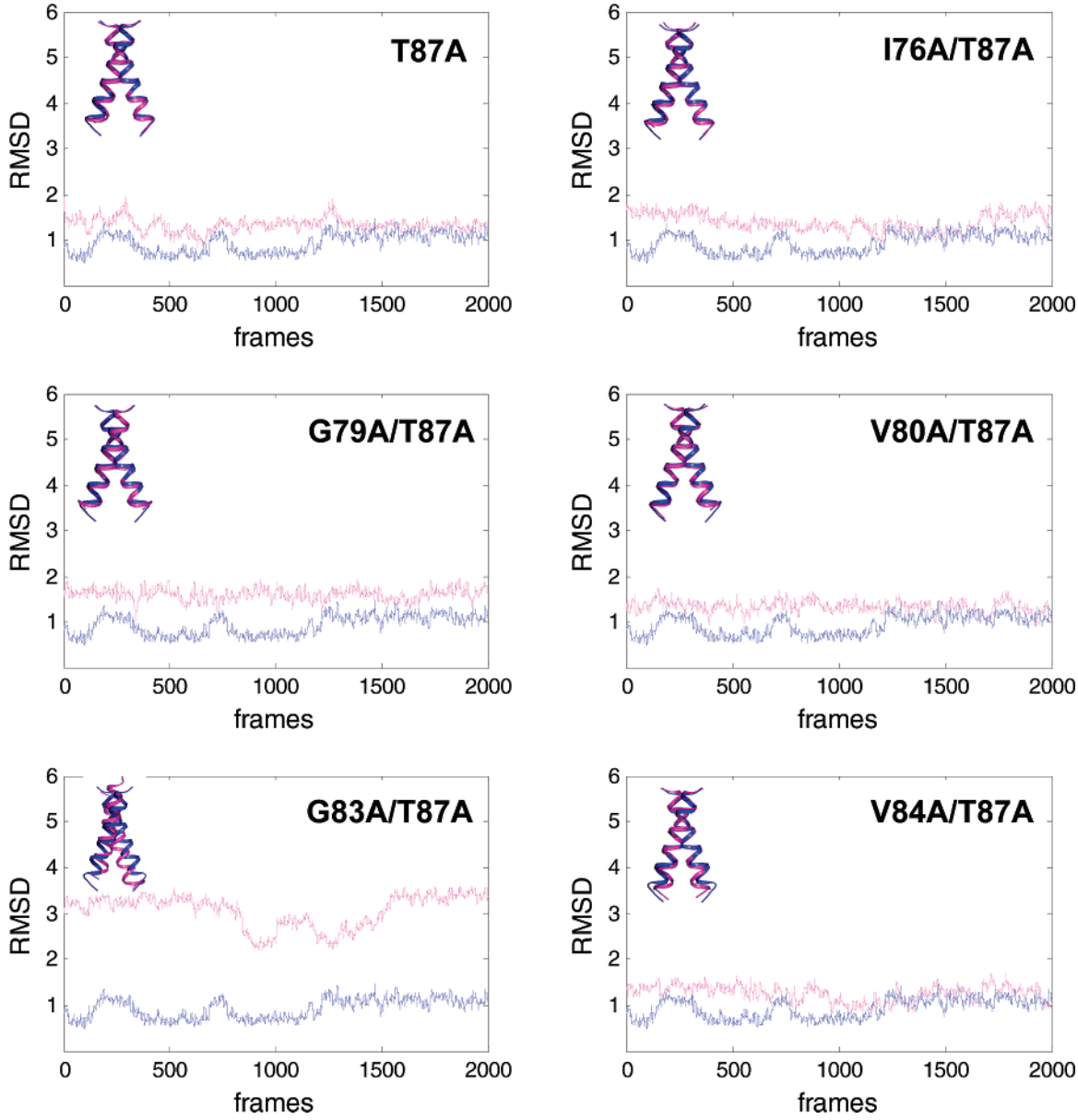

Figure 5. The 1 ns MD trajectories of the wild type (blue) and the T87A series of mutants (magenta). Different from the one reported in Figure 3, the trajectory of the wild type reported in these panels has been obtained by MD simulations with weak distance restraints between the hydroxy oxygen atom of T87 from one helix and the backbone oxygen atom of V84 from the other helix. Each panel reports the C_α-rmsd (Å) of each frame with respect to the experimental solid-state NMR structure. Each inset shows a cartoon representation of the average minimized structure of the mutant (magenta) superimposed on the NMR solid-state structure (blue).

principles of helix−helix association in membranes[1,7−14,30−32] and at probing scoring functions and computational protocols for predicting the likely architecture of transmembrane helix dimers[28,29,33−38] or refining the NMR structures.[25]

Most of the computational experiments are essentially concerned with the wild type form of GpA.[25,28,29,33−38] An elegant free energy perturbation study in explicit membrane/water limited to the L75A and I76A GpA mutants represents one of the few examples of in silico estimations of mutational effects on the free energy of GpA helix−helix association.[32] Free energy perturbation calculations are highly demanding in terms of CPU time and, perhaps, are not the most adequate approaches for fast in silico screening of the effects of mutations on the association properties of membrane proteins. Indeed, dimerization of GpA is such that almost all the entropic contributions to the free energy of association can be neglected. This is the main reason why simple helix−helix interaction descriptors computed on the wild type and mutated forms of the NMR structure of the GpA dimer with no energy minimization,[39] or refined by very limited (1 ps) MD simulations followed by energy minimization,[11−13] proved effective in estimating the dimerization propensities of GpA mutants. In great detail, computational mutational analysis on the GpA system demonstrated that three structure-based empirical parameters, which described steric clashes, favorable van der Waals interactions, and rotamer freedom, were able to reproduce the qualitative dimerization propensities of more than 100 hydrophobic single-point mutants (and 30 insertion mutants) of the GpA transmembrane domain.[39] The main inferences from the regression analysis between such empirical parameters and the dimerization propensities of single-point GpA mutants were that (a) the hydrophobic effect plays a negligible role in the association of transmembrane helices and (b) helix−lipid and lipid−lipid interaction enthalpies as well as peptide and lipid rotational, translational, and conformational entropies are not responsible for the modulation of the thermodynamics of association

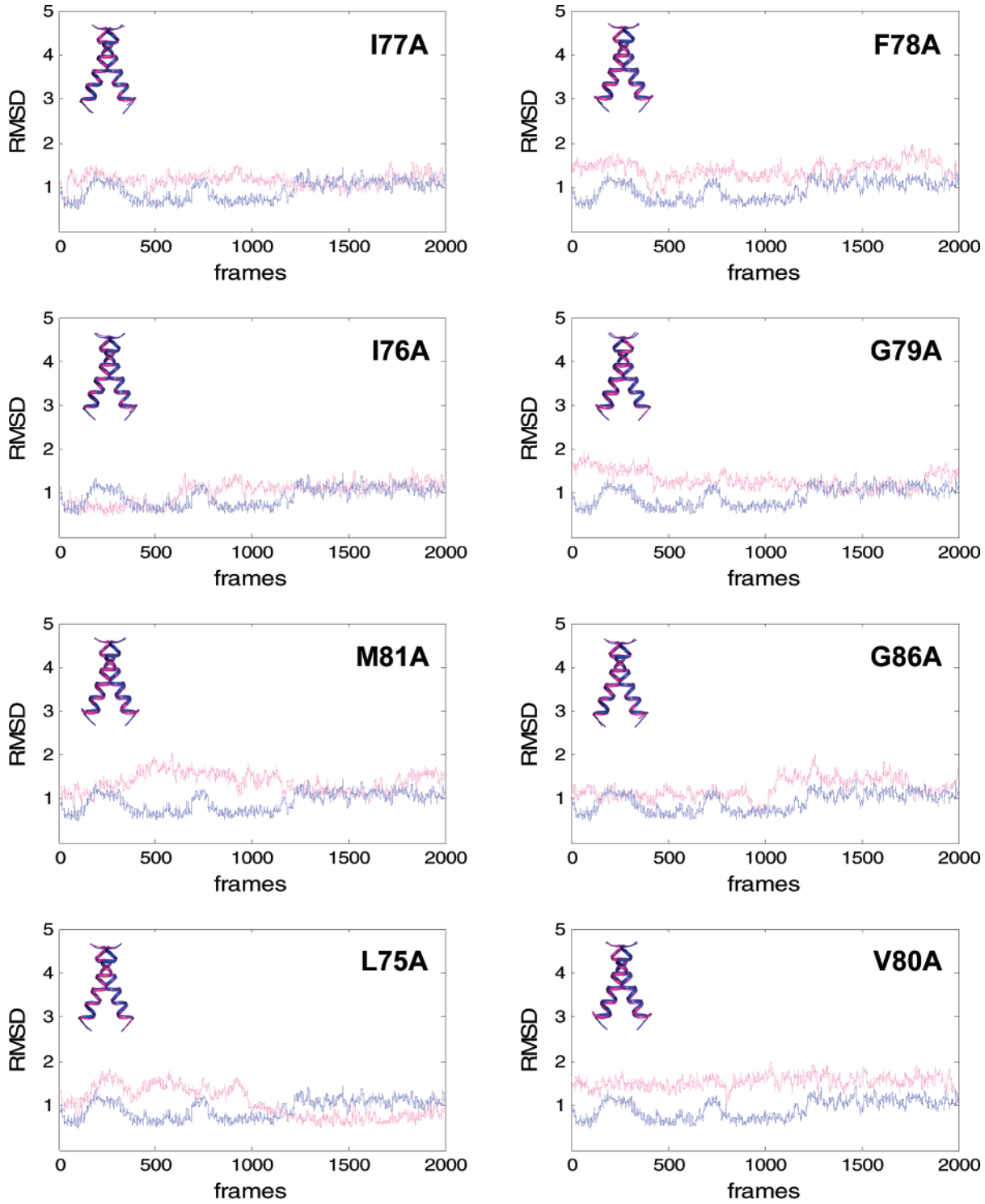

Figure 6. The 1 ns MD trajectories using distance restraints between the hydroxy oxygen atom of T87 from one helix and the backbone oxygen atom of V84 from the other helix (see the text for details). The panels refer to the wild type and selected GpA mutants that, under the effect of these restraints, retain the interhelical hydrogen bonds in the average minimized structures. Each panel reports the C_α-rmsd (Å) of each frame with respect to the experimental solid-state NMR structure. Each inset shows a cartoon representation of the average minimized structure of the mutant (magenta) superimposed on the NMR solid-state structure (blue).

following mutation. Moreover, the loss in side-chain entropy is minimal for the Gly-rich interface.[7] Beside the major role played by the two G79 and G83 residues, which lack side chains, and one Val residue, which adopts only a single low-energy rotamer in helices, the loss in conformational entropy of the remaining side chains in the interfacial region (L75, I76, and T87) is expected to be relatively small.[7] Along the same line, a structural parametrization computed by the occluded surface algorithm and consisting of (a) favorable interchain occluded surface, (b) unfavorable interchain occluded surface, and (c) exposed surface gave significant correlations with the relative free energy of GpA mutants.[11−13] A remarkable inference from these quantitative structure−activity relationship (QSAR) analyses was that changes in van der Waals interactions account for the majority of mutational effects on the thermodynamics of GpA dimerization.[11−13]

The computational mutational analysis of dimeric GpA done in this study represents a good compromise between highly

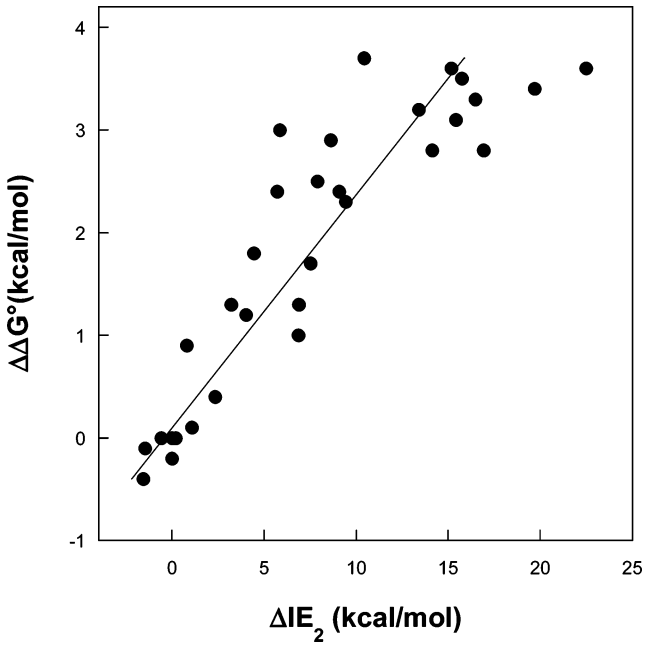

Figure 7. Correlation between experimental relative affinities and relative interaction energies. In these correlations, for all the mutants except for the G83A and T87A series, the IE values have been calculated on the average minimized structures holding interhelical hydrogen bonds as the result of restrained MD simulations. The correlation equation is $\Delta\Delta G^\circ = -0.4(\pm 0.2) + 0.18(\pm 0.02)\ \Delta IE_2$; $N = 31$, $R = 0.89$, $p < 0.0001$, $s = 0.6$.

demanding free energy perturbation calculations and QSAR models based on empirical parameters computed on the static structures of wild type and mutated dimers. In fact, herein mutational analysis of 33 GpA forms has been carried out in parallel by two different computational approaches, i.e., rigid-body docking starting from the monomer and MD simulations on preformed complexes of the wild type and the mutants.

The rigid-body docking-based approach proved effective in reconstituting the native architecture of the GpA dimer for the wild type and the wild-type-like mutants. Indeed, for these forms, at least one of the three docking runs ranked a nativelike solution among the first 10 solutions out of 4000 (Table 1), suggesting that the native helix−helix packing is suitable for these GpA forms. In contrast, for the mutants significantly impaired in dimerization, such as the single and double mutants involving G83, nativelike solutions were found at significantly higher rank numbers and were fewer than those of the wild type and wild-type-like mutants. This suggests that the nativelike packing interactions characterizing the wild type are less suitable for these mutants compared to non-native interactions. In line with these results, the ΔZD-s gave good linear correlations with $\Delta\Delta G^\circ$ (Figure 2), suggesting that changes in the shape complementarity, related to the enthalpic contribution of van der Waals interactions, are essentially responsible for mutation-induced modulation of helix−helix association. Moreover, and consistent with previous studies,[39] neglecting helix rotational, translational, and conformational entropy as well as desolvation does not affect the correlative models, thus proving the acceptability of such approximations. The concept that mutational effects are essentially accounted for by van der Waals interactions,[11−13] which contribute to the enthalpy of association, is consistently supported by the good correlative models between the ΔIE computed on the average minimized structures achieved by MD simulations and $\Delta\Delta G^\circ$ (Figures 2 and 7). Indeed, for most of the 33 GpA forms considered in this study, the van der Waals contribution represents more than 90% of the total IE.

In summary, both the ΔZD-s and ΔIE intermolecular interaction descriptors computed, respectively, on the nativelike docking solutions and on the average minimized structures from MD simulations account for more than 80% of the association free energy changes caused by GpA mutations. These results support the assumption that transmembrane helices associate as rigid bodies and the observed changes in the association free energy following mutation are essentially ascribed to differences in the packing interactions. These inferences are supported by plenty of in vitro studies on helix association in membranes. In this respect, a number of in silico[32] and in vitro[40] experiments support the conformational stability of hydrophobic helices in lipid bilayers. They are also in line with the proposed two-stage model of membrane protein folding,[5,6] which has been further refined and extended.[4] Other support of these assumptions comes from in vitro evidence that membrane proteins fold with a significantly smaller loss in conformational entropy than water-soluble proteins.[1] The loss of backbone entropy is, in fact, significantly decreased because the helices are preformed in the unfolded state.[1,4]

Consistent with the results of rigid-body docking, MD simulations show that the structures of the mutants involving G83 reach the highest C_α-rmsd's from the solid-state NMR structure of the wild type, compared to all other mutants. Moreover, MD simulations show that alanine substitution for G83 propagates the structural perturbation from the mutation site to both the intracellular and extracellular ends of the helix−helix interface (Figures 3 and 4). These results strengthen the knowledge that a glycine at position 83 of GpA is essential for the achievement of the proper helix−helix packing architecture,[7] and that G83 is the most important GpA glycine in this respect. A remarkable result of MD simulations, strikingly consistent with in vitro experiments,[11] is that the majority of the double mutants, especially those that involve G83, show a significant attenuation of the disruptive packing tendency of the single G83A mutant (Table 1 and Figures 3 and 4). In fact, the propagation of the disruptive effect on helix−helix packing shown by the G83A mutation diminishes significantly following the association of the G83A mutant with less disruptive mutations (Table 1 and Figures 3 and 4). This effect is marked by the diminished C_α-rmsd's from the native structure shown by the double mutants compared to the single G83A mutant (Table 1). Such a C_α-rmsd reduction is related to the restoring of native packing interactions lost by the G83A mutant (Figure 4).

The solid-state NMR structure is characterized by the presence of a weak interhelical H-bond between the hydroxy hydrogen atom of T87 from segment A and the carbonyl oxygen atom of V84 from segment B, and vice versa.[9] These polar interactions are absent in the solution NMR structure, which differs from the solid-state structure in the tilt angle and the consequent helix−helix packing architecture.[7,9] Such discrepancies between the two different NMR structures reflect an unclear role of threonines in mediating helix−helix association and stabilizing GpA packing by interhelical H-bonds.[31,41−45] In this study, we have also investigated whether the effects of T87 replacement could be related to the loss of interhelical H-bonds. Consistent with the results of MD simulations in implicit membrane/water models already reported,[28,29] the unrestrained MD simulations on the wild type and mutant structures done in this study resulted in changes of the starting interhelical H-bonds between T87 and V84 into intrahelix H-bonds between T87 and G83 in both helices. However, we found that, in the mutants other than those that involve G83 and T87, the

introduction of weak interhelical distance restraints between T87 and V84 maintains the initial interhelical H-bonds. The presence of such weak H-bonds in the average minimized structures of the wild type and of selected mutants improves the ability of the ΔIE index to account for the effects of the T87 mutation on the binding $\Delta\Delta G°$ (Table 1 and Figures 2 and 7). Thus, the results of this study suggest that the effects of the T87A mutation on the free energy of association are due, at least in part, to the loss of an interhelical H-bond.

Conclusions

The results of this study corroborate the already demonstrated efficiency of the ZDOCK algorithm and scoring function in predicting the supramolecular architecture of transmembrane α-helical proteins.[23] Furthermore, it extends to protein−protein association in membrane the computational method based on the average ZDOCK scores, which was already employed to estimate mutational effects on the association thermodynamics of water-soluble systems.[17−19,26] This suggests that the rigid-body approximation is suitable for handling helix association in membrane. The good performance of the correlative models derived by rigid-body docking stands in the employment of docking scores averaged over the nativelike solutions rather than the scores of single solutions. Indeed, the average scores overcome, at least in part, the low resolution of the complexes involving the modeled mutants and take into account possible changes in the binding modes of the mutant structures compared to the wild type. The performance of the rigid-body docking-based approach is only slightly lower compared to that based on MD simulations. However, the former is significantly faster than the latter and is suitable for preliminary fast screenings of mutational effects on the thermodynamics of helix−helix association. To add interpretative power to the computational models, atomistic simulations that account for protein flexibility are needed. The MD-based models achieved in this study are exemplar in this respect. Indeed, they provided a structural interpretation of the detrimental effect of the G83A mutation on the native helix−helix packing and of the ability of poorly disruptive mutations to attenuate the impairing effect of the G83A mutation when associated to it. Furthermore, the MD-based models provided insight into the role of the native interhelical H-bonds made by T87 and into the effects of T87A and G83A mutations on the dimerization properties of GpA. Collectively, the results of this study support the effectiveness of the selected MD simulation protocol and of the GBSW implicit membrane/water model in handling the effects of single and double mutations on the association properties of transmembrane helices.

In conclusion, the computational approaches presented in this study constitute simple and promising tools for in silico screening of mutational effects on the association properties of integral membrane proteins.

Acknowledgment. This work was supported by Telethon−Italy Grant S00068TELA (to F.F.). We are extremely grateful to Dr. Steven Smith for kindly providing us with the coordinates of the solid-state NMR model of GpA.

References and Notes

(1) DeGrado, W. F.; Gratkowski, H.; Lear, J. D. *Protein Sci.* **2003**, *12*, 647.

(2) Minetti, C. A.; Remeta, D. P. *Arch. Biochem. Biophys.* **2006**, *453*, 32.

(3) Popot, J. L.; Engelman, D. M. *Annu. Rev. Biochem.* **2000**, *69*, 881.

(4) White, S. H.; Wimley, W. C. *Annu. Rev. Biophys. Biomol. Struct.* **1999**, *28*, 319.

(5) Engelman, D. M.; Chen, Y.; Chin, C. N.; Curran, A. R.; Dixon, A. M.; Dupuy, A. D.; Lee, A. S.; Lehnert, U.; Matthews, E. E.; Reshetnyak, Y. K.; Senes, A.; Popot, J. L. *FEBS Lett.* **2003**, *555*, 122.

(6) Popot, J. L.; Engelman, D. M. *Biochemistry* **1990**, *29*, 4031.

(7) MacKenzie, K. R.; Prestegard, J. H.; Engelman, D. M. *Science* **1997**, *276*, 131.

(8) Smith, S. O.; Bormann, B. J. *Proc. Natl. Acad. Sci. U.S.A.* **1995**, *92*, 488.

(9) Smith, S. O.; Song, D.; Shekar, S.; Groesbeek, M.; Ziliox, M.; Aimoto, S. *Biochemistry* **2001**, *40*, 6553.

(10) Brosig, B.; Langosch, D. *Protein Sci.* **1998**, *7*, 1052.

(11) Doura, A. K.; Fleming, K. G. *J. Mol. Biol.* **2004**, *343*, 1487.

(12) Doura, A. K.; Kobus, F. J.; Dubrovsky, L.; Hibbard, E.; Fleming, K. G. *J. Mol. Biol.* **2004**, *341*, 991.

(13) Fleming, K. G.; Ackerman, A. L.; Engelman, D. M. *J. Mol. Biol.* **1997**, *272*, 266.

(14) Fleming, K. G.; Engelman, D. M. *Proc. Natl. Acad. Sci. U.S.A.* **2001**, *98*, 14340.

(15) Fleming, K. G.; Ren, C. C.; Doura, A. K.; Eisley, M. E.; Kobus, F. J.; Stanley, A. M. *Biophys. Chem.* **2004**, *108*, 43.

(16) Mingarro, I.; Whitley, P.; Lemmon, M. A.; von Heijne, G. *Protein Sci.* **1996**, *5*, 1339.

(17) Dell'Orco, D.; De Benedetti, P. G.; Fanelli, F. *BMC Struct. Biol.* **2007**, *7*, 37.

(18) Dell'Orco, D.; Seeber, M.; De Benedetti, P. G.; Fanelli, F. *J. Chem. Inf. Model.* **2005**, *45*, 1429.

(19) Fanelli, F.; Ferrari, S. *J. Struct. Biol.* **2006**, *153*, 278.

(20) Chen, R.; Li, L.; Weng, Z. *Proteins* **2003**, *52*, 80.

(21) Chen, R.; Weng, Z. *Proteins* **2002**, *47*, 281.

(22) Chen, R.; Weng, Z. *Proteins* **2003**, *51*, 397.

(23) Casciari, D.; Seeber, M.; Fanelli, F. *BMC Bioinf.* **2006**, *7*, 340.

(24) Im, W.; Brooks, C. L., III. *Proc. Natl. Acad. Sci. U.S.A.* **2005**, *102*, 6771.

(25) Cuthbertson, J. M.; Bond, P. J.; Sansom, M. S. *Biochemistry* **2006**, *45*, 14298.

(26) Dell'Orco, D.; De Benedetti, P. G.; Fanelli, F. *From Computational Biophysics to Systems Biology Workshop*; NIC Series 34; 2006; p 67.

(27) Brooks, B. R.; Bruccoleri, R. E.; Olafson, B. D.; States, D. J.; Swaminathan, S.; Karplus, M. *J. Comput. Chem.* **1983**, *4*, 187.

(28) Im, W.; Feig, M.; Brooks, C. L., III. *Biophys. J.* **2003**, *85*, 2900.

(29) Mottamal, M.; Zhang, J.; Lazaridis, T. *Proteins* **2006**, *62*, 996.

(30) Schneider, D.; Engelman, D. M. *J. Mol. Biol.* **2004**, *343*, 799.

(31) Smith, S. O.; Eilers, M.; Song, D.; Crocker, E.; Ying, W.; Groesbeek, M.; Metz, G.; Ziliox, M.; Aimoto, S. *Biophys. J.* **2002**, *82*, 2476.

(32) Henin, J.; Pohorille, A.; Chipot, C. *J. Am. Chem. Soc.* **2005**, *127*, 8478.

(33) Bu, L.; Im, W.; Brooks, C. L., III. *Biophys. J.* **2007**, *92*, 854.

(34) Fleishman, S. J.; Ben-Tal, N. *J. Mol. Biol.* **2002**, *321*, 363.

(35) Chen, Z.; Xu, Y. *Proteins* **2006**, *62*, 539.

(36) Akula, N.; Pattabiraman, N. *J. Biomol. Struct. Dyn.* **2005**, *22*, 625.

(37) Efremov, R. G.; Vereshaga, Y. A.; Volynsky, P. E.; Nolde, D. E.; Arseniev, A. S. *J. Comput.-Aided Mol. Des.* **2006**, *20*, 27.

(38) Pappu, R. V.; Marshall, G. R.; Ponder, J. W. *Nat. Struct. Biol.* **1999**, *6*, 50.

(39) MacKenzie, K. R.; Engelman, D. M. *Proc. Natl. Acad. Sci. U.S.A.* **1998**, *95*, 3583.

(40) Yano, Y.; Takemoto, T.; Kobayashi, S.; Yasui, H.; Sakurai, H.; Ohashi, W.; Niwa, M.; Futaki, S.; Sugiura, Y.; Matsuzaki, K. *Biochemistry* **2002**, *41*, 3073.

(41) Choma, C.; Gratkowski, H.; Lear, J. D.; DeGrado, W. F. *Nat. Struct. Biol.* **2000**, *7*, 161.

(42) Eilers, M.; Shekar, S. C.; Shieh, T.; Smith, S. O.; Fleming, P. J. *Proc. Natl. Acad. Sci. U.S.A.* **2000**, *97*, 5796.

(43) Gratkowski, H.; Lear, J. D.; DeGrado, W. F. *Proc. Natl. Acad. Sci. U.S.A.* **2001**, *98*, 880.

(44) Russ, W. P.; Engelman, D. M. *J. Mol. Biol.* **2000**, *296*, 911.

(45) Zhou, F. X.; Merianos, H. J.; Brunger, A. T.; Engelman, D. M. *Proc. Natl. Acad. Sci. U.S.A.* **2001**, *98*, 2250.